PCCP

Accepted Manuscript

ROYAL SOCIETY OF CHEMISTRY

www.rsc.org/pccp

An impurity intermediate band due to Pb doping induced promising thermoelectric performance of $Ca_5In_2Sb_6$

Zhenzhen Feng[1], Yuanxu Wang[1,2,a], Yuli Yan[1], Guangbiao Zhang[1], Jueming Yang[1], Jihua Zhang[1,2], Chao Wang[1]

[1]*Institute for Computational Materials Science, School of Physics and Electronics, Henan University, Kaifeng 475004, People's Republic of China and*

[2]*Guizhou Provincial Key Laboratory of Computational Nano-Material science, Guizhou Normal College, Guiyang 550018, People's Republic of China*

(Dated: May 11, 2015)

Abstract

Band engineering is one of the effective approaches for designing ideal thermoelectric materials. Introducing an intermediate band in the band gap of semiconducting thermoelectric compounds may largely increase the carrier concentration and improve the electrical conductivity of these compounds. We test this hypothesis by Pb doping in Zintl $Ca_5In_2Sb_6$. In the current work, we have systematically investigated the electronic structure and thermoelectric performances of substitutional doping with Pb on In sites at a doping level of 5% (0.2 e/cell) for $Ca_5In_2Sb_6$ by using density functional theory combined with semi-classical Boltzmann theory. It is found that in contrast to Zn doping, Pb doping introduces a partially filled intermediate band in the band gap of $Ca_5In_2Sb_6$, which originates from the Pb s states by weakly hybridizing with the Sb p states. Such an intermediate band dramatically increases the electrical conductivity of $Ca_5In_2Sb_6$ and has little detrimental effect on its Seebeck coefficient, which may increase its thermoelectric figure of merit, ZT. Interestingly, a maximum ZT value of 2.46 may be achieved at 900 K for crystalline Pb-doped $Ca_5In_2Sb_6$ when the carrier concentration is optimized. Therefore, Pb-doped $Ca_5In_2Sb_6$ may be a promising thermoelectric material.

Keywords: Zintl; $Ca_5In_2Sb_6$; Pb doping; Thermoelectric properties.

[a] E-mail: wangyx@henu.edu.cn

I. INTRODUCTION

Thermoelectric materials for converting waste heat into usable electrical energy have attracted great attention in recent years.[1, 2] A central focus has been to improve the performance of materials to enable new applications. The efficiency of thermoelectric devices is limited by a material-dependent figure of merit $ZT = S^2\sigma T/\kappa$, where S is the Seebeck coefficient (also known as the thermopower), σ is the electrical conductivity, T is the absolute temperature, and κ is the thermal conductivity, which is typically written as the sum of the electronic (electrons and holes transporting heat) and lattice (phonon traveling through the lattice) contributions: $\kappa = \kappa_e + \kappa_l$. This limits the efficiency of thermoelectric power generation to a few percent. Finding practical materials with high performance is challenging because the transport coefficients entering ZT have opposite dependencies on the parameters of the materials. For example, a high σ value does not normally occur in conjunction with high S and low κ_l values, which implies that strong phonon scattering does not normally occur in materials with high σ. These conundrums have impeded the applications of thermoelectric materials.[3–5] During the past several years, intense research effort has been devoted to improving the ZT for high energy conversion efficiency in current complex bulk thermoelectric materials.[6, 7] This has led to a new concept: a "phonon-glass electron-crystal (PGEC)", [8–10] which is embodied in the use of rattling modes and nanostructure to separately modify electron and phonon transport and optimize S and σ in materials with unusual electronic structures, such as strongly nonparabolic bands or mixtures of heavy and light bands structures. The development of novel thermoelectric materials with special structures that can tune electron and phonon transport in a relatively independent way is clearly needed for enhancing performance, which is required for eventual large-scale applications of thermoelectric materials.

Zintl phase compounds provide a good balance between high power factor and low thermal conductivity, and consequently, they are prime candidates for applying the PGEC concept to obtain high-ZT thermoelectric materials. With the Zintl-Klemm-Busmann concept,[11] the donation of valence electrons from the cations (alkali, alkaline earth or rare earth) to the polyanionic sub-lattice, which in turn forms covalent bonds to satisfy the valence requirement, is assumed to be complete. The degree of electron transfer between cations and anions[12] has well-documented influence on the transport properties of Zintl

compounds.[13–15] The need to satisfy valence often leads to a complex structure. Such a complex crystal structure can strongly scatter phonons, resulting in a low lattice thermal conductivity, so many Zintl phase compounds naturally have "phonon glass" behavior.[16, 17] At the same time, the complex, covalent structures can potentially be harnessed for electronic conduction, leading to the desired "electron crystal" behavior.[18, 19] Moreover, good thermoelectric performance is generally found in heavily doped semiconductors with carrier concentrations on the order of 10^{19} to 10^{21} carriers per cm^3, which can be easily realized because the rich solid-state chemistry of the Zintl phase enables numerous opportunities to modify the fundamental transport parameters to enhance thermoelectric performance.

Complex Zintl phase materials appear to be promising candidates for thermoelectric applications.[20–22] Among $A_5M_2Pn_6$ (A = divalent alkaline earth or rare earth metals; M = triels; Pn = pnictogen elements) compounds, most form either $Ca_5Ga_2Sb_6$ or $Ba_5Al_2Bi_6$ structures.[23, 24] Several $Ca_5Ga_2Sb_6$ Zintl compounds have been the focus of both experimental and computational studies.[25–29] The structure of $Ca_5In_2Sb_6$ is isotypic with that of $Ca_5Ga_2Sb_6$, which is composed of infinite chains of linked MPn_4 tetrahedra. Compared with $Ca_5Al_2Sb_6$, $Ca_5In_2Sb_6$ exhibited improvements of both electrical and thermal properties, and the mobility of undoped $Ca_5In_2Sb_6$ is nearly twice that of undoped $Ca_5Al_2Sb_6$ at room temperature.[25] Upon optimization of the carrier concentration through Zn doping, $Ca_5In_2Sb_6$ is expected to have an improved peak ZT relative to $Ca_5Al_2Sb_6$.[30] Nevertheless, Zn doping is often used to increase the carrier concentration of Zintl compounds and consequently improve their electrical conductivity. However, the Seebeck coefficient of a Zn-doped Zintl compound decreases largely due to the increased carrier concentration. The band shape of the valence band maximum and conduction band minimum for Zintl compounds changes little with Zn doping, which usually induces the degenerate semiconducting behavior in Zn-doped Zintl compounds. Traditionally, thermoelectric material is a single-band-gap semiconductor in which electrons are directly promoted from the valence band to the conduction band. Thus, high electrical conductivity will occur when a partially filled intermediate band is inserted into the forbidden band gap. The electrons can be excited not only from the valence band to the conduction band but also from the intermediate band to the conduction band and from the valence band to the intermediate band. As the intermediate band is isolated, the material will have a higher electrical conductivity due to the sub-band gap, which will result in a high ZT. Our results show that in Pb-doped $Ca_5In_2Sb_6$,

an intermediate band appears in the band gap. The calculated thermoelectric properties are greatly enhanced compared to that of the host $Ca_5In_2Sb_6$, and a maximum ZT value of 2.46 may be obtained at 900 K for $Ca_5In_{1.9}Pb_{0.1}Sb_6$. Such an enhancement is due to the change of the band structure. Therefore, the Pb-doped $Ca_5In_2Sb_6$ with a doping level of 0.2 e/cell is a potential candidate of band engineering for improving thermoelectric performance.

II. COMPUTATIONAL DETAIL

The orthorhombic structure of $Ca_5Ga_2Sb_6$[31] was taken as the initial bulk model to be relaxed to find the minimum energy structure. The structure was optimized using the Vienna *ab initio* simulation package (VASP) based on density functional theory.[32–37] The projector augmented wave (PAW) method of Blöchl[38] with the implementation of Kresse and Joubert was used. The Perdew-Burke-Ernzerh parametrization of generalized-gradient approximation (PBE-GGA) was used for the exchange correlation potential. A plane-wave cutoff energy of 500 eV was employed throughout, and for the Brillouin zone integrations of $Ca_5In_2Sb_6$, k-point sampling was employed, with $7 \times 8 \times 15$ points chosen. The stopping criterion of convergence for electronic self-consistent interactions is a total energy within 10^{-6} eV. The calculations were performed by relaxing the positions of both atoms and lattice constants to find the most stable crystal structure. The crystal structure is considered to be in equilibrium when the Hellmann-Feynman forces on each ion are less than 0.005 eV/Å and the maximum stress is less than 0.02 GPa.

The electronic structures of $Ca_5In_2Sb_6$ were then calculated using the full-potential linearized augmented plane waves method,[39] as implemented in WIEN2k.[40–42] The modified semi-local Becke-Johnson exchange correlation potential (TB-mBJ)[43] was used, which has been known to give much more accurate band gaps than the standard Engel-Vosko generalized-gradient approximation (EV-GGA).[44] The muffin-tin radii were chosen to be 2.5 a.u. for Ca, In, and Sb. The cutoff parameter $R_{mt} \times K_{max} = 9$ (K_{max} is the magnitude of the largest k vector) was used, and the self-consistent calculations were performed with 1000 k-points in the irreducible Brillouin zone; the total energy is converged to within 0.0001 Ry. The Seebeck coefficient and electrical conductivity were then calculated using semi-classical Boltzmann theory[45, 46] within the constant scattering time approximation, as implemented in the Boltz-Trap code.[47] This approximation, which has commonly been ap-

plied to many thermoelectric materials, including degenerately doped semiconductors, Zintl phases, and oxides,[48, 49] is based on the assumption that the scattering time determining the electrical conductivity does not vary strongly with energy on the scale of kT. The constant scattering time approximation has been used to calculate the transport coefficients of some known thermoelectric materials, and a very good agreement was found with experimental results.[22, 28, 46, 50, 51] To study the electronic structure and thermoelectric properties of $Ca_5In_{1.9}Pb_{0.1}Sb_6$, we constructed a $1 \times 1 \times 5$ supercell of $Ca_5In_2Sb_6$ and then replaced one In atom with a Pb atom in a 130-atom cell, which corresponded to a 5% (0.2 e/cell) dopant concentration. To understand the effect of Pb content on the electronic structure and transport properties of Pb-doped $Ca_5In_2Sb_6$, we also calculated the electronic structure and transport properties of $Ca_5In_{1.8}Pb_{0.2}Sb_6$ with a $1 \times 1 \times 5$ supercell model, in which the shortest Pb-Pb distances are as long as possible. We also investigated the electronic structure with Zn doping at an In site with a doping level of 5%; this was done by forming a $1 \times 1 \times 5$ supercell with one In atom substituted by a Zn atom. The structures were optimized using VASP with similar choices of parameters. The electronic structures were then calculated with WIEN2k, and the muffin-tin radii were chosen to be 2.5 a.u. for Pb and Zn. Other parameters were in accord with the calculation of $Ca_5In_2Sb_6$.

To determine whether Pb substitution for In sites is more favorable energetically, we calculated the formation energies ($\triangle E$) of Pb-doped $Ca_5In_2Sb_6$. The doping formation energy is estimated by using the following formula:

$$\triangle E = E_{doping} + E_A - E_{pure} - E_{Pb}, \quad (1)$$

where E_{doping} and E_{pure} are the total energies of the doped and pure $Ca_5In_2Sb_6$ species, respectively, at their most stable states. A represents Ca, In, and Sb. E_{Ca}, E_{In}, E_{Sb}, E_{Pb} are the total energies per atom for Ca-face-centered cubic, In-tetragonal, Sb-rhombohedral, Pb-face-centered cubic structures, respectively. The calculated formation energy for $Ca_5In_{1.9}Pb_{0.1}Sb_6$ (0.69 eV) is lower than that for $Ca_{4.9}Pb_{0.1}In_2Sb_6$ (1.84 eV, 1.84 eV, and 1.93 eV for Pb substituting for Ca1, Ca2, and Ca3 sites, respectively) and $Ca_5In_2Sb_{5.9}Pb_{0.1}$ (1.40 eV, 1.64 eV, and 0.94 eV for Pb substituting for Sb1, Sb2, and Sb3 sites, respectively). Thus, the Pb atom prefers to occupy the In site rather than the Ca site or the Sb site in Pb-doped $Ca_5In_2Sb_6$.

III. RESULTS AND DISCUSSION

A. Crystal structure

Fig. 1 shows the optimized structures of $Ca_5In_2Sb_6$ viewed from different directions. There are 10 Ca atoms, 4 In atoms, and 12 Sb atoms in each unit cell. The structure contains seven crystallographically unique atoms - three Ca, one In, and three Sb. The three nonequivalent Ca sites are referred to as "Ca1"(four atoms), "Ca2"(four atoms), and "Ca3"(two atoms), and the three nonequivalent Sb sites are referred to as "Sb1"(four atoms), "Sb2"(four atoms), and "Sb3"(four atoms). Structural and bond parameters of the optimized $Ca_5In_2Sb_6$ are shown in Table I and Table II, respectively. $Ca_5In_2Sb_6$ can be expressed as $Ca_5^{+2}In_2^{-1}Sb_4^{-1}Sb_2^{-2}$. The two In atoms are each bonded to four Sb atoms, which have a valence of -1; two $Sb1^{1-}$ are shared between two $InSb_4$ tetrahedra and two $Sb2^{2-}$ are bonded to one In atom, while the two $Sb3^{1-}$ ions connect the adjacent chains. Fig. 1(a) shows the structure of $Ca_5In_2Sb_6$ viewed down the c-axis, and Fig. 1(b) shows the one-dimensional covalent substructure, in which the $InSb_4$-tetrahedra chains are connected by Sb-Sb bonds. From Fig. 1(a), we can see that the basic repeat unit of $Ca_5In_2Sb_6$ is two-tetrahedra units $[In_2Sb_6]^{10-}$. The repeat units form the layered structure along the c direction which is conducive to the transport of electrons, without considering the Ca atoms. These two-tetrahedra units in $Ca_5In_2Sb_6$ lead to a large unit cell, with 26 atoms, and low lattice thermal conductivity.[25]

B. Electrical transport properties

The electrical transport properties of $Ca_5In_2Sb_6$ were calculated by combining the semi-classical Boltzmann transport theory under constant relaxation time approximation and *ab initio* band structure. The rigid-band approach was used to calculate the transport properties of different doping levels. For metals or degenerate semiconductors (parabolic band, energy-independent scattering approximation), the Seebeck coefficient is given by Eq. (2).[52] The electrical conductivity (σ) is related to the carrier concentration (n) which through the carrier mobility μ, is defined as Eq. (3).

$$S = \frac{8\pi^2 k_B^2}{3eh^2} m^*_{DOS} T (\frac{\pi}{3n})^{\frac{2}{3}}, \quad (2)$$

$$\sigma = ne\mu, \tag{3}$$

where m^*_{DOS} is the density of states effective mass, k_B is Boltzmann's constant, e is the charge of an electron, and h is Planck's constant. The carrier mobility (μ) is strongly affected by the band mass of a single valley (m^*_b): $\mu \propto 1/m^{*5/2}_b$. The relation between the density-of-states effective mass and the band mass of a single valley is $m^*_{DOS} = {N_v}^{2/3} m^*_b$,[53, 54] where N_v is the band degeneracy. The explicit forms of Eq. (2) suggest that the Seebeck coefficient is the proportional to the temperature and density of states effective mass but inversely related to the carrier concentration. Eq. (3) suggests that the electrical conductivity is proportional to the carrier concentration and inversely proportional to the effective mass. As previously mentioned, a good thermoelectric material requires a large Seebeck coefficient and a high electrical conductivity. Hence, we have studied the thermoelectric properties of $Ca_5In_2Sb_6$ as a function of carrier concentration to achieve a good balance between the Seebeck coefficient and the electrical conductivity. However, the calculated result of $\frac{\sigma}{\tau}$ includes the scattering time τ. We used the experimental data in Ref. [30] to obtain the value of τ. To obtain more accurate electrical conductivities, the relaxation time τ was calculated with an experimental electrical resistivity of $\rho = 6.7855$ mΩ cm at 600 K in the doping concentration of x = 0.05 and a carrier concentration of n = 1.694×10^{20} cm^{-3}. At the same carrier concentration, the calculated $\frac{\sigma}{\tau}$ is 5.57×10^{18} $(\Omega \text{ms})^{-1}$ at 600 K. By comparing the calculated $\frac{\sigma}{\tau}$ with the experimental electrical resistivity at the same doping level, we can obtain $\tau = 2.646 \times 10^{-15}$ s for this sample of $Ca_5In_2Sb_6$ at 600 K. τ decreases as the temperature increases over the entire range, which shows a T^{-1} dependence. For the doping dependence, there is a standard electron-phonon interaction relaxation time, $\tau \propto n^{-1/3}$.[51] This yields $\tau = 8.842 \times 10^{-6}\ T^{-1} n^{-1/3}$ with τ in s, T in K, and n in cm^{-3}. With the calculated relaxation time, we can obtain the electrical conductivity at different carrier concentrations and temperatures. To simulate the ZT value, we assume that the thermal conductivity at the same temperature is constant at different carrier concentrations. The thermal conductivities of $Ca_5In_2Sb_6$ at 300 K, 500 K, 700 K, and 900 K that we used are 1.4 W/mK, 1.02 W/mK, 0.83 W/mK, and 0.8 W/mK, respectively.[30]

Fig. 2 depicts the logarithmic dependence of the Seebeck coefficient, S, electrical conductivity, σ, and figure of merit, ZT, of p-type and n-type $Ca_5In_2Sb_6$ on carrier concentration from 10^{19} cm^{-3} to 10^{21} cm^{-3} at 300 K, 500 K, 700 K, and 900 K. The combined Seebeck

coefficient is given by[55]

$$S = \frac{S_e\sigma_e + S_h\sigma_h}{\sigma_e + \sigma_h}, \tag{4}$$

$$S_h = \frac{k_B}{e}[ln(\frac{N_v}{n_p}) + 2.5 - \gamma], \tag{5}$$

$$S_e = -\frac{k_B}{e}[ln(\frac{N_c}{n_n}) + 2.5 - \gamma], \tag{6}$$

where γ is the scattering mechanism parameter, S_e (S_h) is the Seebeck coefficient of electrons (holes), σ_h (σ_e) is the electrical conductivity of holes (electrons), N_v (N_c) is the effective density of states in the valence band (conduction band), n_p is the number of holes, and n_n is the number of electrons. As seen from Fig. 2(a), the Seebeck coefficient of p-type $Ca_5In_2Sb_6$ is positive, while that of n-type is negative, which is in agreement with Eq. (5) and Eq. (6), respectively. The values of S decrease with increasing carrier concentration and increase with increasing temperature at high carrier concentration, which can be explained by Eq. (2). The S of n-type $Ca_5In_2Sb_6$ is larger than that of the p-type one. From Fig. 2(b), the electrical conductivity is proportional to the carrier concentration, which is consistent with Eq. (3). However, σ decreases from 300 K to 500 K, 700 K, and eventually to 900 K, which is mainly because the motion of the carriers is impeded by the increased lattice vibration with increasing temperature. Fig. 2(c) shows the estimated figure of merit ZT as a function of the carrier concentration. As seen in Fig. 2(c), for p-type $Ca_5In_2Sb_6$, the maximum ZT can reach 0.38 at 900 K, corresponding to the carrier concentration of 1.03×10^{20} cm^{-3}. For n-type $Ca_5In_2Sb_6$, the maximum ZT can reach 0.49 at 900 K, corresponding to a carrier concentration of 1.16×10^{20} cm^{-3}.

To investigate the most favorable direction for transport properties of $Ca_5In_2Sb_6$, we also calculated the transport properties as a function of carrier concentration from 10^{19} cm^{-3} to 10^{21} cm^{-3} along the x, y, and z directions at 900 K using the Boltzmann theory, as shown in Fig. 3. As seen from Fig. 3(a), the Seebeck coefficients along the x direction are larger than those for the other two directions at a high carrier concentration for both p-type and n-type $Ca_5In_2Sb_6$, owing to their smaller dispersion along the x direction, as shown in the calculated band structure. Fig. 3(b) shows the electrical conductivities of $Ca_5In_2Sb_6$ as a function of carrier concentration along the three directions. From Fig. 3(b), we can see that the electrical conductivities of p-type and n-type $Ca_5In_2Sb_6$ along the z direction are larger than those along the x and y directions. This results from the different dispersions of the

valence band and the conduction band along Y - S, Y - Γ, and Y - T. σ along the z direction for p-type $Ca_5In_2Sb_6$ is larger than that of the n-type one, which will cause p-type $Ca_5In_2Sb_6$ to have a larger σ than that of n-type $Ca_5In_2Sb_6$ at high temperatures (Fig. 2(b)). The reason that σ along the z direction for p-type $Ca_5In_2Sb_6$ is larger than that for the n-type one will be described in detail below in Fig. 6. As seen in Fig. 3(c), for n-type $Ca_5In_2Sb_6$, the maximum ZT along the z direction is equal to 0.64, with a carrier concentration of 8.57 $\times$ 10^{19} electrons per cm^3. Meanwhile, the maximum ZT of p-type $Ca_5In_2Sb_6$ along the z direction is 1.12, corresponding to the carrier concentration of 1.03 $\times$ 10^{20} holes per cm^3. Therefore, good thermoelectric performance along the z direction for $Ca_5In_2Sb_6$ is predicted.

C. Electronic structure

The electronic structure is crucial for analyzing the transport properties. The relation between electronic structure and thermoelectric figure of merit ZT can be defined by Hicks and Dresselhaus.[56] ZT increases with an inherent parameter B in anisotropic three-dimensional single-band circumstances when the thermal and electrical currents travel in a certain direction. The inherent parameter B and maximum attainable figure of merit (Z_{max}) are defined by:

$$B = \frac{1}{3\pi^2}(\frac{2K_BT}{\hbar^2})^{3/2}(m_x^* m_y^* m_z^*)^{1/2}\frac{K_B^2 T\mu}{ek_l}, \tag{7}$$

$$Z_{max} \propto \gamma\frac{T^{3/2}\tau_z\sqrt{\frac{m_x^* m_y^*}{m_z^*}}}{k_l}e^{(r+1/2)}, \tag{8}$$

where γ is the degeneracy of band extrema, $m_i^*(i{=}x, y, z)$ is the effective mass of the carriers (electrons or holes) in the ith direction, τ_z is the relaxation time of the carriers moving along the transport (z) direction, and r is the scattering parameter. μ is the carrier mobility along the transport direction and k_l is the lattice thermal conductivity.

Eq. (7) and (8) suggest that a high ZT value is benefited from a large effective mass, a high carrier mobility, a low lattice thermal conductivity, and high degeneracy of band extrema. Electronic structure calculations can directly provide important information regarding these properties. Hence, we calculated the band structure, band decomposed charge density, and density of states (DOS) of $Ca_5In_2Sb_6$. Because the transport properties are closely related to the electronic states near the valence band maximum (VBM) and conduc-

tion band minimum (CBM), we only focus on the electronic states near the Fermi level. As shown in Fig. 4, $Ca_5In_2Sb_6$ is a semiconductor with a nearly direct band gap of 0.49 eV. The band dispersion relationship determines the effective mass (m^*), which is given by:

$$m^* = \hbar^2 [\frac{d^2E(k)}{dk^2}]^{-1}_{E(k)=E_f}, \quad (9)$$

where k is the wave vector and $\hbar$ is the Planck constant divided by 2π. The calculated band effective masses are m_x^* = - 2.35 m_e (along Y - S), m_y^* = - 1.2 m_e (along Y - Γ), and m_z^* = - 0.5 m_e (along Y - T) for the valence band. We know that the light band is beneficial for large electrical conductivity and that a heavy band or large degeneracy can result in high Seebeck coefficients. Therefore, we can understand the anisotropic of the transport properties of p-type $Ca_5In_2Sb_6$ shown in Fig. 3.

To further explain the transport, we calculated the partial charge densities near the Fermi level of $Ca_5In_2Sb_6$ using VASP. The VBM charge densities at point Y are shown in Fig. 5(a) and (c), and the displayed isosurface levels are 0.002 and 0.0012, respectively. The CBM charge densities at point Y are shown in Fig. 5(b) and (d), and the displayed isosurface levels are 0.0016 and 0.0012, respectively (the unit of charge density is e/Å^3). Fig. 5(a) shows that the VBM mainly consists of electrons around Sb atoms, which have the following order: Sb3 > Sb1 > Sb2. However, as shown in Fig. 5(b), the Sb and Ca atoms dominate the CBM. These results can provide guidance for further investigating the doping effect on $Ca_5In_2Sb_6$ with the appropriate atoms. When we set the isosurface level at a value of 0.0012, the Ca1 and Sb2 atoms are connected by charge density for p-type $Ca_5In_2Sb_6$ along the z direction (Fig. 5(c)). However, for n-type $Ca_5In_2Sb_6$, all of the atoms are not yet connected by charge density (Fig. 5(d)). This result demonstrates that the electrical conductivity for p-type $Ca_5In_2Sb_6$ should be larger than that of n-type $Ca_5In_2Sb_6$ along the z direction (Fig. 3(b)).

Fig. 6 shows the projected electronic DOS for $Ca_5In_2Sb_6$. The projected DOS shows that the upper valence band is mainly dominated by Sb states and that the conduction band bottom mainly comes from Sb and Ca states, which is in accordance with the calculated partial charge densities in Fig. 5. Moreover, the In orbitals contribute to the lower valence band and the upper conduction band, which make almost no contribution to the states near the Fermi level for electrical transport. In this regard, doping on the In sites could not only increase the DOS near the Fermi level but also optimize the carrier concentration. On the

one hand, such electronic structure characteristics make it possible for $Ca_5In_2Sb_6$ to still be used as electron-crystal materials when doped, and on the other hand, the alloying on the In site can scatter phonons and will reduce thermal conductivity.

D. Pb-doped $Ca_5In_2Sb_6$

Doping in the Zintl phases is an effective strategy to optimize ZT. Zn-doped $Ca_5In_2Sb_6$ has been previously reported, and the results of the experiment showed that the maximum figure of merit obtained in optimally Zn-doped $Ca_5In_2Sb_6$ is 0.7 at 1000 K.[30] Fig. 7 shows our calculated band structure of $Ca_5In_{1.9}Zn_{0.1}Sb_6$ along the high symmetry directions in the Brillouin zone of the supercell. As seen from Fig. 7, the E_F level is located inside the valence band, as would be expected for a degenerate semiconductor. The band shape of VBM and CBM for Zintl compounds changes little due to Zn doping, which induces the degenerate semiconducting behavior in $Ca_5In_{1.9}Zn_{0.1}Sb_6$. Zn doping is always used to increase the carrier concentration of Zintl compounds and consequently improve their electrical conductivity. However, the Seebeck coefficient of Zn-doped Zintl compounds decreases largely due to the increased carrier concentration.

Therefore, it is valuable to explore a new method for increasing the electrical conductivity of Zintl compounds with little or no decrease in their Seebeck coefficient. Thus, we investigate the electronic structure and transport performances with Pb doping at In sites with a doping level of 5% for $Ca_5In_2Sb_6$. The calculated band structure and corresponding DOS for the $Ca_5In_{1.9}Pb_{0.1}Sb_6$ supercell are shown in Fig. 8. Because the $1 \times 1 \times 5$ supercell model was used to calculate the band structure of $Ca_5In_{1.9}Pb_{0.1}Sb_6$, the original bands along Γ - Z and T - Y will be folded five times to yield the bands in Fig. 8(a). As seen from Fig. 8(a), the most obvious change in the band structure with the doping of the Pb ion is the appearance of an additional intermediate band in the band gap. The intermediate band is contributed by the Pb s states. It can be seen from Fig. 4 and Fig. 8(a) that the Pb dopant does not change the valence band of the host material. The intermediate band induced by the Pb doping divided the main band gap into two sub-band gaps and therefore may benefit the thermoelectric performance. The main gap for Pb-doped $Ca_5In_2Sb_6$ is 0.55 eV, with a little broadening, which can be explained by the energy level repulsion between the intermediate band and the conduction band maximum. We can see

that the band degeneracy at the top of the valence band is equals to 2, while the bottom of the conduction band is equal 1, which is conducive to obtain large Seebeck coefficients for p-type $Ca_5In_{1.9}Pb_{0.1}Sb_6$. Moreover, the valence bands and conduction bands along the Y - T direction have a stronger dispersion than those along the other two directions. Thus, n-type and p-type $Ca_5In_{1.9}Pb_{0.1}Sb_6$ may have a larger electrical conductivity along the z direction than along the x and y directions. Because of the appearance of the intermediate band, electrons can be excited not only from the valence band to the conduction band but also from the intermediate band to the conduction band and from the valence band to the intermediate band, which will lead to a very large electrical conductivity as shown in Fig. 9(b). To uncover the origin of the intermediate band, we show the DOS in Fig. 8(b). As seen in this figure, the intermediate band mainly comes from the Pb s states, with small contributions of the Sb p states reflecting the weak hybridization between the Pb and Sb ions. Because the Sb s states make little contribution to this intermediate band, we do not show the Sb s states in this figure. In $Ca_5In_2Sb_6$, the four nearest neighboring Sb atoms around the In atom form a tetrahedral crystal field. The Pb ion is substituted for the In atom in $Ca_5In_2Sb_6$ and is therefore located in the tetrahedral crystal field environment. The top of the valence bands is dominated by Sb p states, while the conduction band bottom originates from the Pb s states, Pb p states, and Ca d states. Thus, Pb plays an important role for the transmission of electrons, which causes $Ca_5In_{1.9}Pb_{0.1}Sb_6$ to have a relatively large electrical conductivity, leading to a large ZT for $Ca_5In_{1.9}Pb_{0.1}Sb_6$.

The semi-classical Boltzmann transport theory was used under the electron relaxation time approximation for studying electrical transport properties. With a constant relaxation time, the Seebeck coefficient, as a function of carrier concentration, can be directly obtained without adjustable parameters. Conversely, the electrical conductivity and figure of merit can be obtained using an estimated relaxation time. We used the experimental data[30] to estimate the relaxation time, which yields $\tau = 6.876 \times 10^{-5}\, T^{-1} n^{-1/3}$, with τ in s, T in K, and n in cm^{-3}. With the calculated relaxation time, we can obtain the electrical conductivity at different carrier concentrations and temperatures. Fig. 9 shows the logarithmic dependence of the Seebeck coefficient, S, electrical conductivity, σ, and figure of merit, ZT, of p-type and n-type $Ca_5In_{1.9}Pb_{0.1}Sb_6$ on carrier concentration from 2.5×10^{20} cm^{-3} to 10^{21} cm^{-3} at 300 K, 500 K, 700 K, and 900 K. As seen in Fig. 9(a), the Seebeck coefficients decrease with increasing doping levels or carrier concentration. Moreover, at a fixed doping level,

the Seebeck coefficients increase with increasing temperature. As seen by comparing Fig. 2(b) with Fig. 9(b), the electrical conductivity of $Ca_5In_{1.9}Pb_{0.1}Sb_6$ increases greatly, which can be explained by the band structure (Fig. 8). σ of the p-type $Ca_5In_{1.9}Pb_{0.1}Sb_6$ is larger than that of the n-type one. The calculated ZT of the p-type $Ca_5In_{1.9}Pb_{0.1}Sb_6$ is larger than that of the n-type one at the optimum carrier concentration (Fig. 9(c)) due to the larger electrical conductivity of p-type $Ca_5In_{1.9}Pb_{0.1}Sb_6$. For p-type $Ca_5In_{1.9}Pb_{0.1}Sb_6$, the maximum ZT can reach 0.87, 1.7, 2.33, and 2.46 at 300 K, 500 K, 700 K, and 900 K, corresponding to the carrier concentration of 3.49×10^{20} holes per cm^3, 3.48×10^{20} holes per cm^3, 3.66×10^{20} holes per cm^3, and 3.85×10^{20} holes per cm^3, respectively. For n-type $Ca_5In_{1.9}Pb_{0.1}Sb_6$, the maximum ZT can reach 0.71, 1, 0.99, and 1.01 at 300 K, 500 K, 700 K, and 900 K, corresponding to the carrier concentration of 2.86×10^{20} electrons per cm^3, 2.97×10^{20} electrons per cm^3, 2.8×10^{20} electrons per cm^3, and 3.45×10^{20} electrons per cm^3, respectively. Thus, a good thermoelectric performance for $Ca_5In_{1.9}Pb_{0.1}Sb_6$ can be predicted.

To understand the effect of Pb content on the electronic structure and transport properties of Pb-doped $Ca_5In_2Sb_6$, we also calculated the electronic structure and transport properties with Pb doping at the In sites, with a doping level of 10% (0.4 e/cell) for $Ca_5In_2Sb_6$. The calculated band structure and corresponding DOS for $Ca_5In_{1.8}Pb_{0.2}Sb_6$ are shown in Fig. 10. As seen in Fig. 10, the intermediate bands contains two isolated bands. As seen in Fig. 10(b), the intermediate bands mainly come from the hybridized Pb s states and Sb p states. Because the Sb s states make little contribution to these intermediate bands, we do not show the Sb s states in this figure. It is to say that the increasing of Pb doping may lead to a strong hybridization between Pb s and Sb p orbitals. Moreover, we estimated the relaxation time using the same method, which yields $\tau = 2.07 \times 10^{-4}\ T^{-1}n^{-1/3}$, with τ in s, T in K, and n in cm^{-3}. Compared with undoped $Ca_5In_2Sb_6$, the Seebeck coefficient of $Ca_5In_{1.8}Pb_{0.2}Sb_6$ decreases greatly (Fig. 11(a)), and the electrical conductivity increases (Fig. 11(b)). As shown in Fig. 11(c), for p-type $Ca_5In_{1.8}Pb_{0.2}Sb_6$, the maximum ZT can reach 1.24 at 900 K, corresponding to the carrier concentration of 7.89×10^{20} holes per cm^3. For n-type $Ca_5In_{1.8}Pb_{0.2}Sb_6$, the maximum ZT can reach 0.87 at 900 K, corresponding to the carrier concentration of 7.82×10^{20} electrons per cm^3.

Consequently, different from Zn doping, Pb doping with a doping level of 5% may dramatically increase the electrical conductivity of $Ca_5In_2Sb_6$ and has little detrimental effect on

its Seebeck coefficient. Therefore, a high ZT value can be achieved in Pb-doped $Ca_5In_2Sb_6$.

IV. CONCLUSION

In summary, engineering the electronic band structure of $Ca_5In_2Sb_6$ by substitutional doping with Pb at In sites may improve the thermoelectric properties of this material. High ZT values originate from the appearance of an intermediate band in the band gap of $Ca_5In_2Sb_6$. Such an isolated intermediate band, with an optimal position, is mainly due to the Pb s states, with small contributions from the Sb p states for $Ca_5In_{1.9}Pb_{0.1}Sb_6$. The intermediate band will dramatically increase the electrical conductivity of $Ca_5In_2Sb_6$ and has little detrimental effect on its Seebeck coefficient. Therefore, the ZT value of $Ca_5In_2Sb_6$ may be greatly enhanced by doping with Pb at In sites with doping level of 5%. For p-type $Ca_5In_{1.9}Pb_{0.1}Sb_6$, the maximum ZT can reach 2.46 at 900 K, with a carrier concentration of 3.85×10^{20} holes per cm^3. Moreover, n-type $Ca_5In_{1.9}Pb_{0.1}Sb_6$ can achieve a ZT value of 1.01 at 900 K, corresponding to a carrier concentration of 3.45×10^{20} electrons per cm^3. Thus, the current work will motivate future experimental work for improving the thermoelectric performance of Zintl compounds by Pb doping.

V. ACKNOWLEDGMENTS

This research was sponsored by the National Natural Science Foundation of China (grant Nos. U1204112, 51371076), and the Program for Innovative Research Team (in Science and Technology) in University of Henan Province (grant No. 13IRTSTHN017).

[1] M. S. Dresselhaus, G. Chen, M. Y. Tang, R. Yang, H. Lee, D. Wang, Z. Ren, J.-P. Fleurial, and P. Gogna, Adv. Mater. **19**, 1043 (2007).

[2] B. Sales, D. Mandrus, and R. K. Williams, Science **272**, 1325 (1996).

[3] M. Zhou, J.-F. Li, and T. Kita, J. Am. Chem. Soc. **130**, 4527 (2008).

[4] R. Yang, G. Chen, and M. S. Dresselhaus, Nano Lett. **5**, 1111 (2005).

[5] X. Ke, C. Chen, J. Yang, L. Wu, J. Zhou, Q. Li, Y. Zhu, and P. R. Kent, Phys. Rev. Lett. **103**, 145502 (2009).

[6] G. J. Snyder and E. S. Toberer, Nat. Mater. **7**, 105 (2008).

[7] J. R. Sootsman, D. Y. Chung, and M. G. Kanatzidis, Angew. Chem. Int. Ed. **48**, 8616 (2009).

[8] D. M. Rowe, *CRC handbook of thermoelectrics* (CRC press, 1995).

[9] A. F. Ioffe and H. J. Goldsmid, *Physics of semiconductors* (Infosearch London, 1960).

[10] T. M. Tritt, Science **283**, 804 (1999).

[11] H. Schäfer, B. Eisenmann, and W. Müller, Angew. Chem. Int. Ed. Engl. **12**, 694 (1973).

[12] R. Sanderson, Science **114**, 670 (1951).

[13] J. Wang, S.-Q. Xia, and X. T. Tao, Inorg. Chem. **51**, 5771 (2012).

[14] C. A. Uvarov, F. Ortega-Alvarez, and S. M. Kauzlarich, Inorg. Chem. **51**, 7617 (2012).

[15] S. Bobev, J. D. Thompson, J. L. Sarrao, M. M. Olmstead, H. Hope, and S. M. Kauzlarich, Inorg. Chem. **43**, 5044 (2004).

[16] E. S. Toberer, A. Zevalkink, and G. J. Snyder, J. Mater. Chem. **21**, 15843 (2011).

[17] F. Seitz and D. Turnbull, *Solid state physics*, Vol. 7 (Academic Press, 1958).

[18] S. M. Kauzlarich, *Chemistry, structure, and bonding of Zintl phases and ions* (VCH New York, 1996).

[19] A. M. Mills, R. Lam, M. J. Ferguson, L. Deakin, and A. Mar, Coord. Chem. Rev. **233**, 207 (2002).

[20] A. Zevalkink, E. S. Toberer, W. G. Zeier, E. Flage-Larsen, and G. J. Snyder, Energy Environ. Sci. **4**, 510 (2011).

[21] A. Zevalkink, W. G. Zeier, G. Pomrehn, E. Schechtel, W. Tremel, and G. J. Snyder, Energy Environ. Sci. **5**, 9121 (2012).

[22] Q. F. Shi, Y. L. Yan, and Y. X. Wang, Appl. Phys. Lett. **104**, 012104 (2014).

[23] G. Cordier, E. Czech, M. Jakowski, and . Schäfer, Rev. Chim. Mineral **18**, 9 (1981).

[24] I. Todorov, D. Y. Chung, L. Ye, A. J. Freeman, and M. G. Kanatzidis, Inorg. Chem. **48**, 4768 (2009).

[25] A. Zevalkink, G. S. Pomrehn, S. Johnson, J. Swallow, Z. M. Gibbs, and G. J. Snyder, Chem. Mater. **24**, 2091 (2012).

[26] E. S. Toberer, A. Zevalkink, N. Crisosto, and G. J. Snyder, Adv. Funct. Mater. **20**, 4375 (2010).

[27] Y. L. Yan and Y. X. Wang, J. Mater. Chem. **21**, 12497 (2011).

[28] Y. L. Yan, Y. X. Wang, and G. B. Zhang, J. Mater. Chem. **22**, 20284 (2012).

[29] S. I. Johnson, A. Zevalkink, and G. J. Snyder, J. Mater. Chem. A **1**, 4244 (2013).

[30] A. Zevalkink, J. Swallow, and G. J. Snyder, Dalton Trans. **42**, 9713 (2013).

[31] P. Verdier, P. l'Haridon, M. Maunaye, and Y. Laurent, Acta Crystallogr. Sect. B **32**, 726 (1976).

[32] D. M. Ceperley and B. Alder, Phys. Rev. Lett. **45**, 566 (1980).

[33] G. Kresse and J. Furthmüller, Phys. Rev. B **54**, 11169 (1996).

[34] G. Kresse and J. Hafner, Phys. Rev. B **47**, 558 (1993).

[35] J. P. Perdew and A. Zunger, Phys. Rev. B **23**, 5048 (1981).

[36] G. Kresse and J. Hafner, J. Phys.: Condens. Matter **6**, 8245 (1994).

[37] G. Kresse and D. Joubert, Phys. Rev. B **59**, 1758 (1999).

[38] P. E. Blöchl, Phys. Rev. B **50**, 17953 (1994).

[39] L. Nordstrom and D. J. Singh, *Planewaves, Pseudopotentials, and the LAPW method* (Springer, 2006).

[40] P. Blaha, K. Schwarz, G. Madsen, D. Kvasnicka, and J. Luitz, Schwarz (Vienna University of Technology, Austria, 2001) (2001).

[41] P. Hohenberg and W. Kohn, Phys. Rev. **136**, B864 (1964).

[42] D. Koelling and B. Harmon, J. Phys. C: Solid State Phys. **10**, 3107 (1977).

[43] F. Tran and P. Blaha, Phys. Rev. Lett. **102**, 226401 (2009).

[44] J. P. Perdew, K. Burke, and M. Ernzerhof, Phys. Rev. Lett. **77**, 3865 (1996).

[45] J. M. Ziman, J. M. Ziman, J. M. Ziman, and G. B. Physicist, *Electrons and phonons: the theory of transport phenomena in solids* (Clarendon Press Oxford, UK, 2001).

[46] G. K. Madsen, K. Schwarz, P. Blaha, and D. J. Singh, Phys. Rev. B **68**, 125212 (2003).

[47] G. K. Madsen and D. J. Singh, Comput. Phys. Commun. **175**, 67 (2006).

[48] D. Parker and D. J. Singh, Phys. Rev. X **1**, 021005 (2011).

[49] L. Xi, Y. Zhang, X. Shi, J. Yang, X. Shi, L. Chen, W. Zhang, J. Yang, and D. J. Singh, Phys. Rev. B **86**, 155201 (2012).

[50] A. T. Ramu, L. E. Cassels, N. H. Hackman, H. Lu, J. M. Zide, and J. E. Bowers, J. Appl. Phys. **107**, 083707 (2010).

[51] K. P. Ong, D. J. Singh, and P. Wu, Phys. Rev. B **83**, 115110 (2011).

[52] M. Cutler, J. Leavy, and R. Fitzpatrick, Phys. Rev. **133**, A1143 (1964).

[53] Y. Pei, X. Shi, A. LaLonde, H. Wang, L. Chen, and G. J. Snyder, Nature **473**, 66 (2011).

[54] G. Mahan, Academic Press, New York **51**, 11 (1998).

[55] M. Chen, J. Appl. Phys. **71**, 3636 (1992).

[56] L. Hicks and M. Dresselhaus, Phys. Rev. B **47**, 12727 (1993).

TABLE I. Lattice constants and atomic coordinates in Wyckoff position of $Ca_5In_2Sb_6$

Lattice parameter	Atomic type	x	y	z
Crystal system: Orthorhombic	Ca1	0.324	0.016	0.000
Space group: Pbam (No.55)	Ca2	0.910	0.753	0.000
a=12.1546Å	Ca3	0.000	0.000	0.000
b=14.3461Å	Sb1	0.164	0.831	0.000
c=4.6202Å	Sb2	0.150	0.092	0.500
	Sb3	0.540	0.096	0.500
	In	0.337	0.214	0.500

TABLE II. Bond distances (in Å) in $Ca_5In_2Sb_6$

Atomic type	Nearest neighbor table			
Ca1	Sb1 3.291	Sb2 3.319	Sb3 3.682	Sb3 3.261
Ca2	Sb1 3.230	Sb2 3.292	Sb3 3.283	
Ca3	Sb1 3.137	Sb2 3.221	Sb3 6.20	Sb3 6.263
In	Sb1 2.856	Sb2 2.876	Sb3 2.994	

FIGURE CAPTIONS

: Fig. 1. Orthorhombic structure of $Ca_5In_2Sb_6$ in space group *Pbam*. Color code: Ca, green; In, blue; Sb, brown.

: Fig. 2. Transport coefficients of *p*-type and *n*-type $Ca_5In_2Sb_6$ as a function of carrier concentration from 10^{19} to 10^{21} cm^{-3} at 300 K, 500 K, 700 K, and 900 K.

: Fig. 3. The anisotropic thermoelectric properties of $Ca_5In_2Sb_6$ as a function of carrier concentration from 10^{19} to 10^{21} cm^{-3} at 900 K.

: Fig. 4. Calculated band structures of $Ca_5In_2Sb_6$. Top of the valence band is set to zero. The special *k* points Γ, Z, T, Y, X, and S represent the points (0, 0, 0), (0, 0, 0.5), (0, 0.5, 0.5), (0, 0.5, 0), (0.5, 0, 0), and (0.5, 0.5, 0), respectively.

: Fig. 5. Calculated band decomposed charge density of $Ca_5In_2Sb_6$ for the bands near the Fermi level; (a) for valence bands at point Y, isosurface value 0.002; (b) for conduction bands at point Y, isosurface value 0.0016; (c) for valence bands at point Y, isosurface value 0.0012; (d) for conduction bands at point Y , isosurface value 0.0012. The unit of charge density is $e/Å^3$.

: Fig. 6. Calculated projected DOS for $Ca_5In_2Sb_6$. The Fermi level is at zero.

: Fig. 7. Calculated band structures of Zn-doped $Ca_5In_2Sb_6$.

: Fig. 8. (a) Calculated band structures of $Ca_5In_{1.9}Pb_{0.1}Sb_6$. (b) Calculated projected DOS for $Ca_5In_{1.9}Pb_{0.1}Sb_6$. The Fermi level is at zero.

: Fig. 9. Transport coefficients of *p*-type and *n*-type $Ca_5In_{1.9}Pb_{0.1}Sb_6$ as a function of carrier concentration from 2.5×10^{20} to 10^{21} cm^{-3} at 300 K, 500 K, 700 K, and 900 K.

: Fig. 10. (a) Calculated band structures of $Ca_5In_{1.8}Pb_{0.2}Sb_6$. (b) Calculated projected DOS for $Ca_5In_{1.8}Pb_{0.2}Sb_6$. The Fermi level is at zero.

: Fig. 11. Transport coefficients of *p*-type and *n*-type $Ca_5In_{1.8}Pb_{0.2}Sb_6$ as a function of carrier concentration from 5×10^{20} to 10^{21} cm^{-3} at 300 K, 500 K, 700 K, and 900 K.

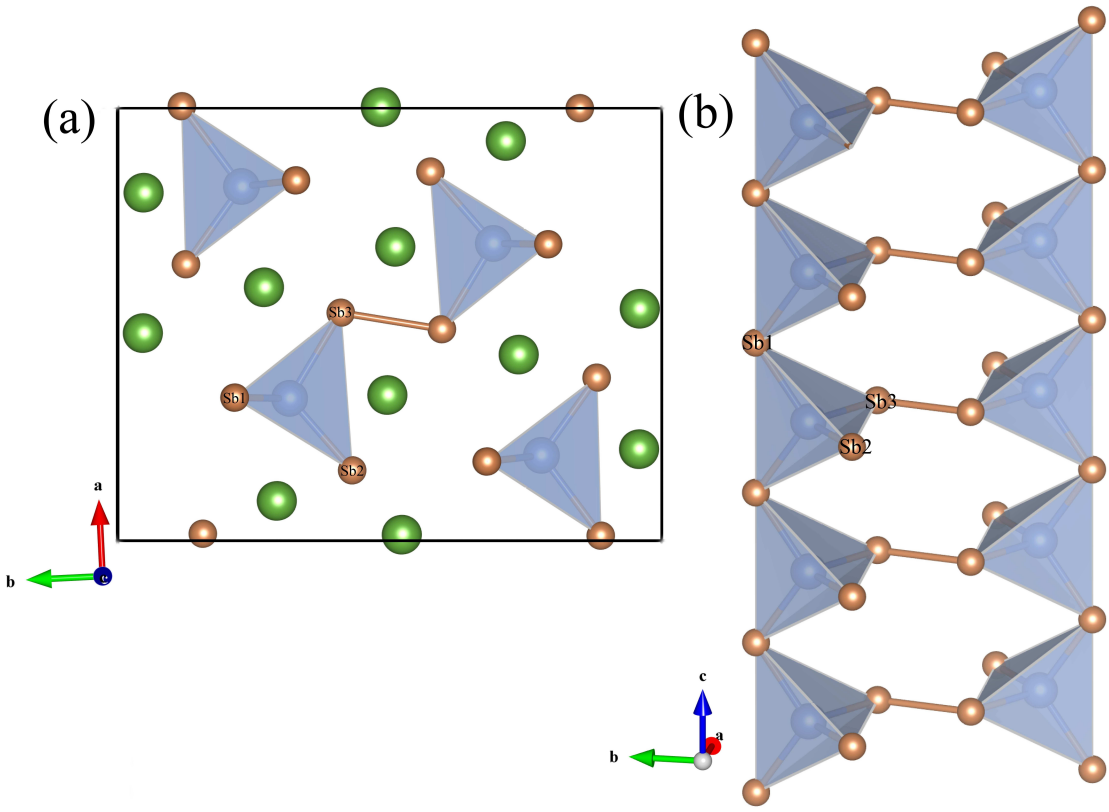

FIG. 1. Orthorhombic structure of $Ca_5In_2Sb_6$ in space group *Pbam*. Color code: Ca, green; In, blue; Sb, brown.

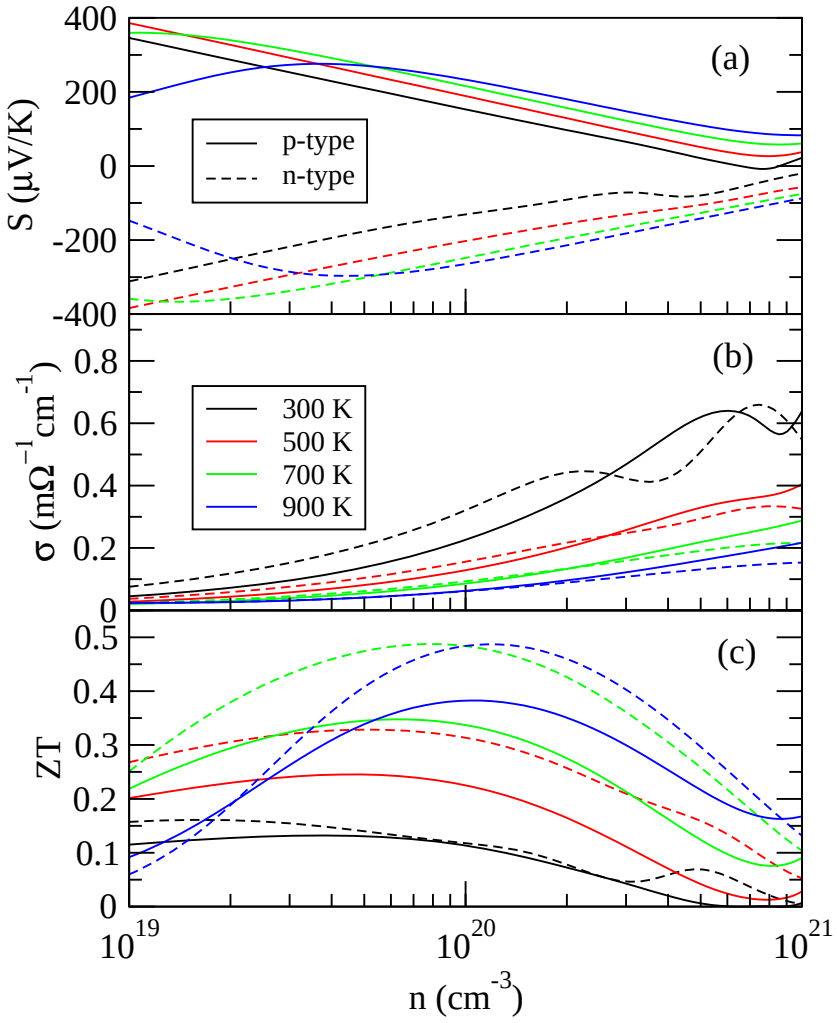

FIG. 2. Transport coefficients of p-type and n-type $Ca_5In_2Sb_6$ as a function of carrier concentration from 10^{19} to 10^{21} cm^{-3} at 300 K, 500 K, 700 K, and 900 K.

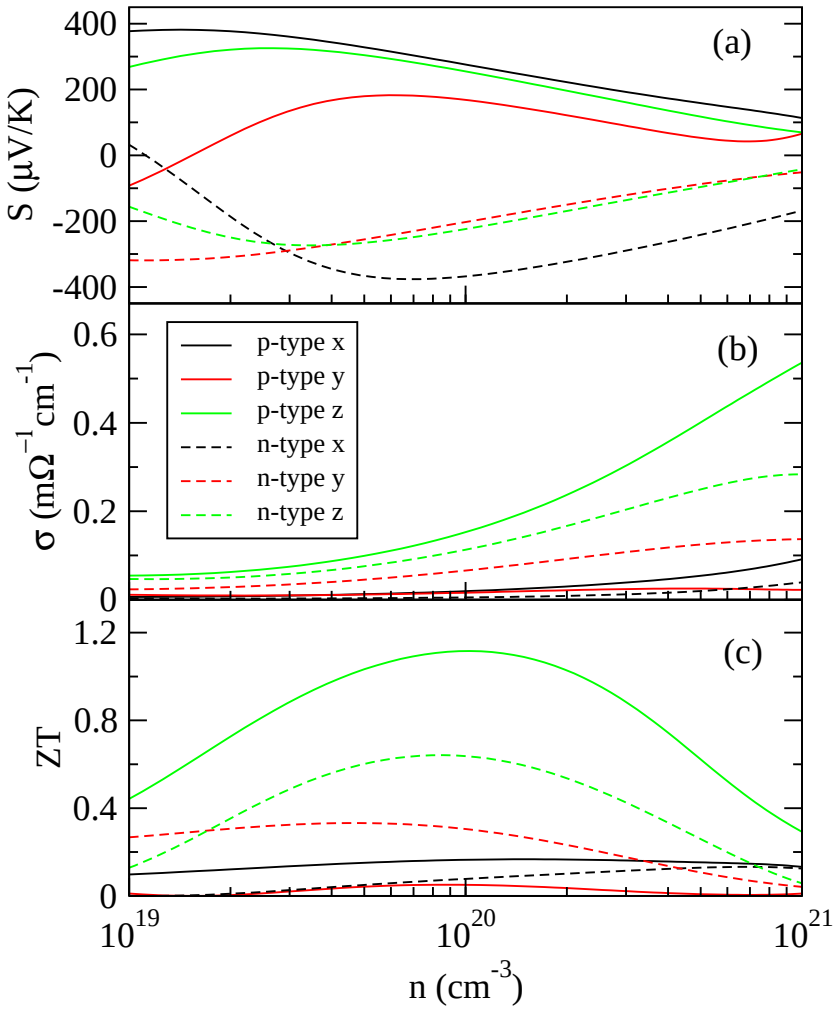

FIG. 3. The anisotropic thermoelectric properties of $Ca_5In_2Sb_6$ as a function of carrier concentration from 10^{19} to 10^{21} cm^{-3} at 900 K.

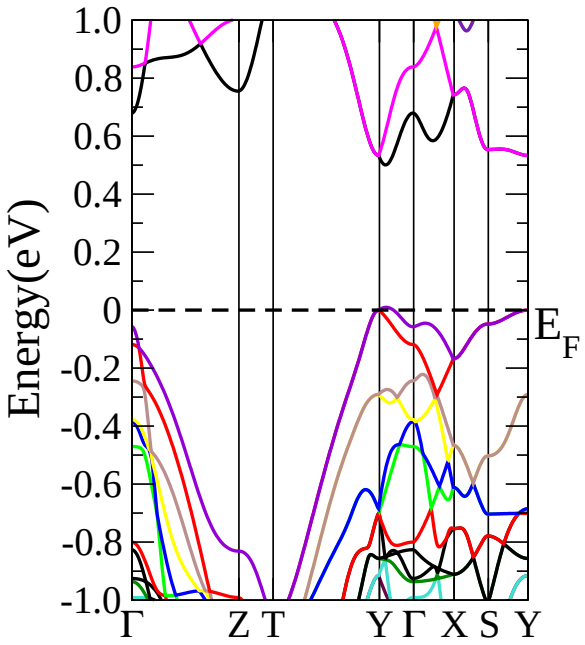

FIG. 4. Calculated band structures of $Ca_5In_2Sb_6$. Top of the valence band is set to zero. The special k points Γ, Z, T, Y, X, and S in the figure represent the points (0, 0, 0), (0, 0, 0.5), (0, 0.5, 0.5), (0, 0.5, 0), (0.5, 0, 0), and (0.5, 0.5, 0), respectively.

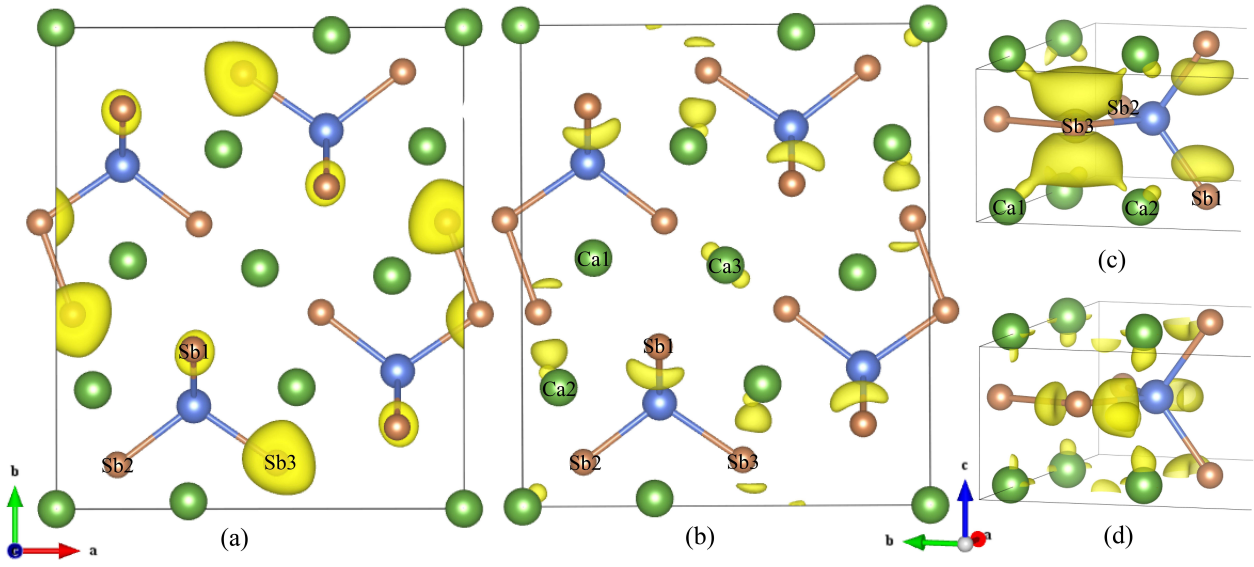

FIG. 5. Calculated band decomposed charge density of $Ca_5In_2Sb_6$ for the bands near the Fermi level; (a) for valence bands at point Y, isosurface value 0.002; (b) for conduction bands at point Y, isosurface value 0.0016; (c) for valence bands at point Y, isosurface value 0.0012; (d) for conduction bands at point Y , isosurface value 0.0012. The unit of charge density is e/Å^3.

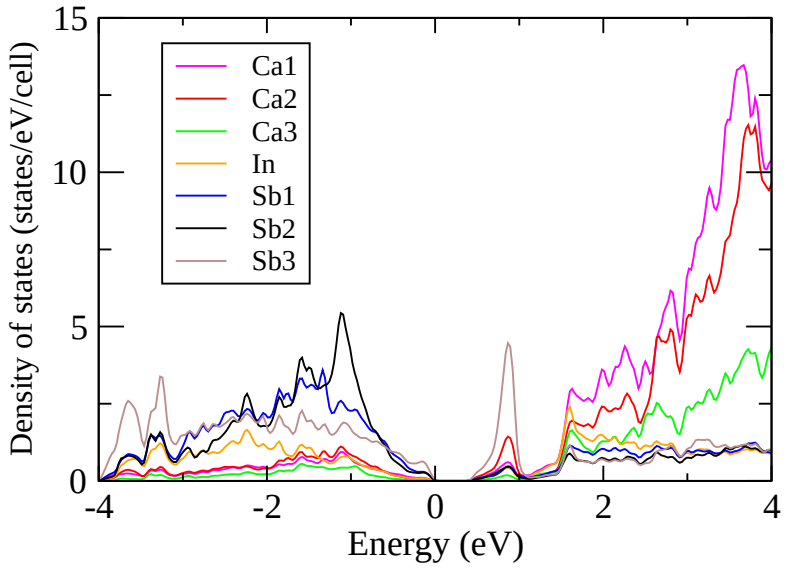

FIG. 6. Calculated projected DOS for $Ca_5In_2Sb_6$. The Fermi level is at zero.

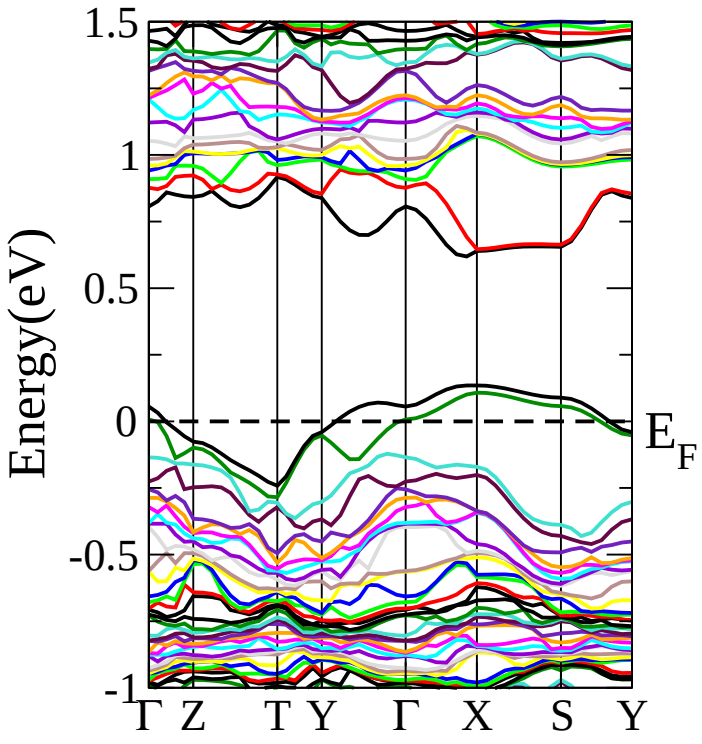

FIG. 7. Calculated band structures of Zn-doped $Ca_5In_2Sb_6$.

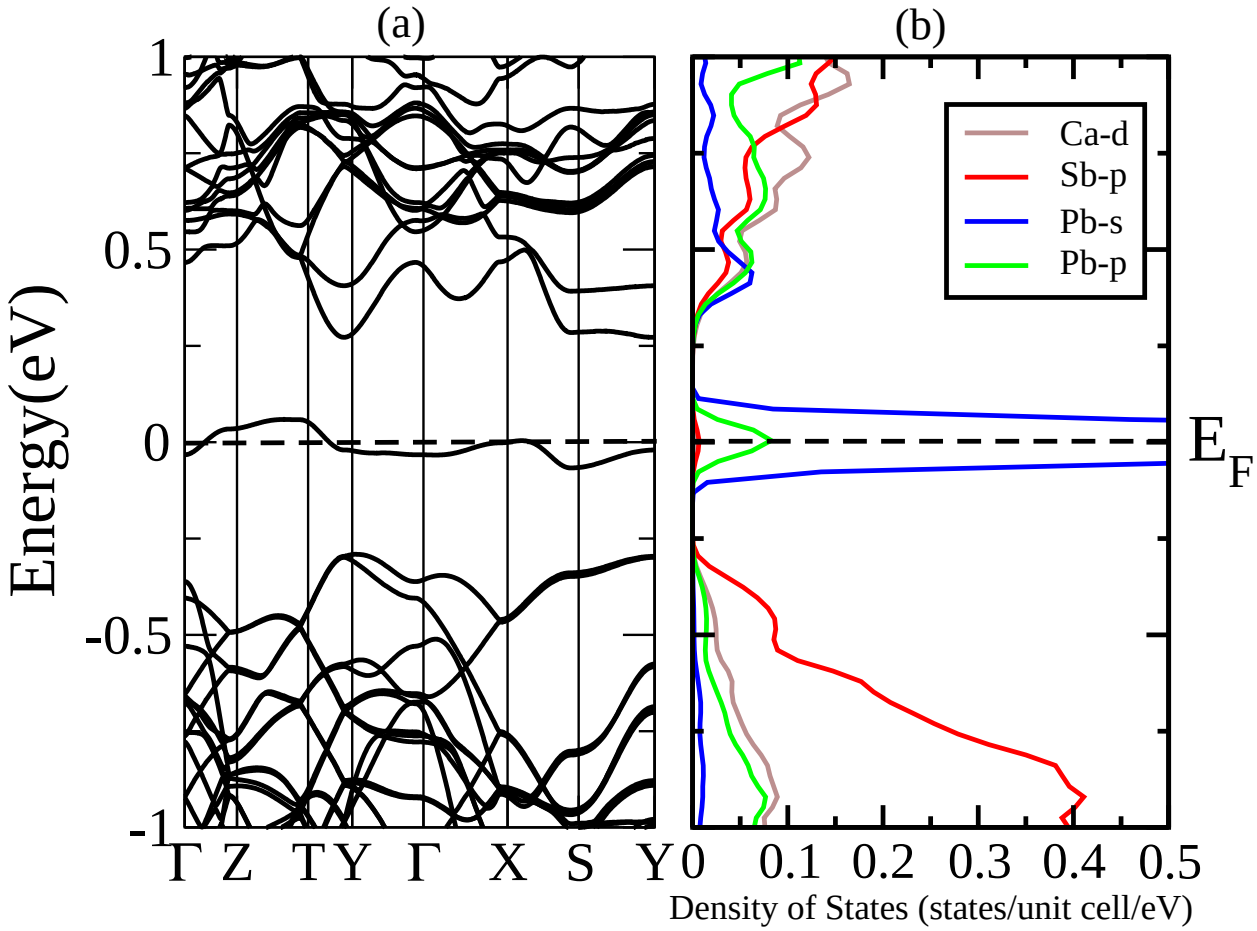

FIG. 8. (a) Calculated band structures of $Ca_5In_{1.9}Pb_{0.1}Sb_6$. (b) Calculated projected DOS for $Ca_5In_{1.9}Pb_{0.1}Sb_6$. The Fermi level is at zero.

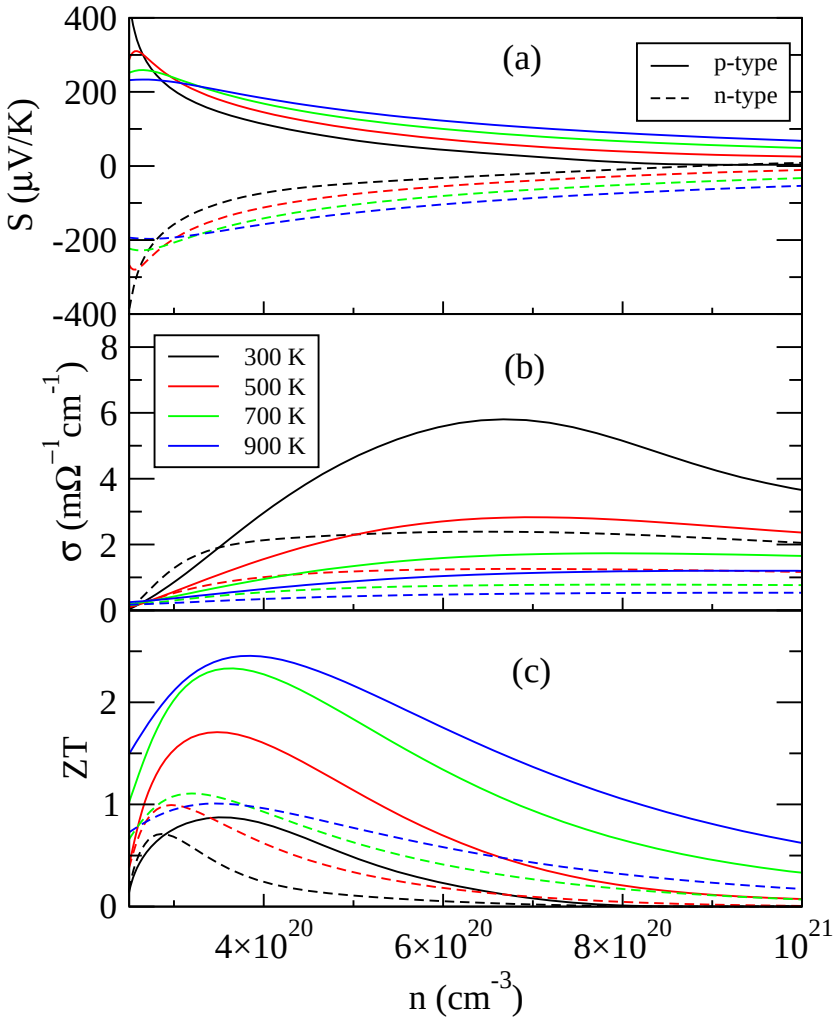

FIG. 9. Transport coefficients of p-type and n-type $Ca_5In_{1.9}Pb_{0.1}Sb_6$ as a function of carrier concentration from 2.5 × 10^{20} to 10^{21} cm^{-3} at 300 K, 500 K, 700 K, and 900 K.

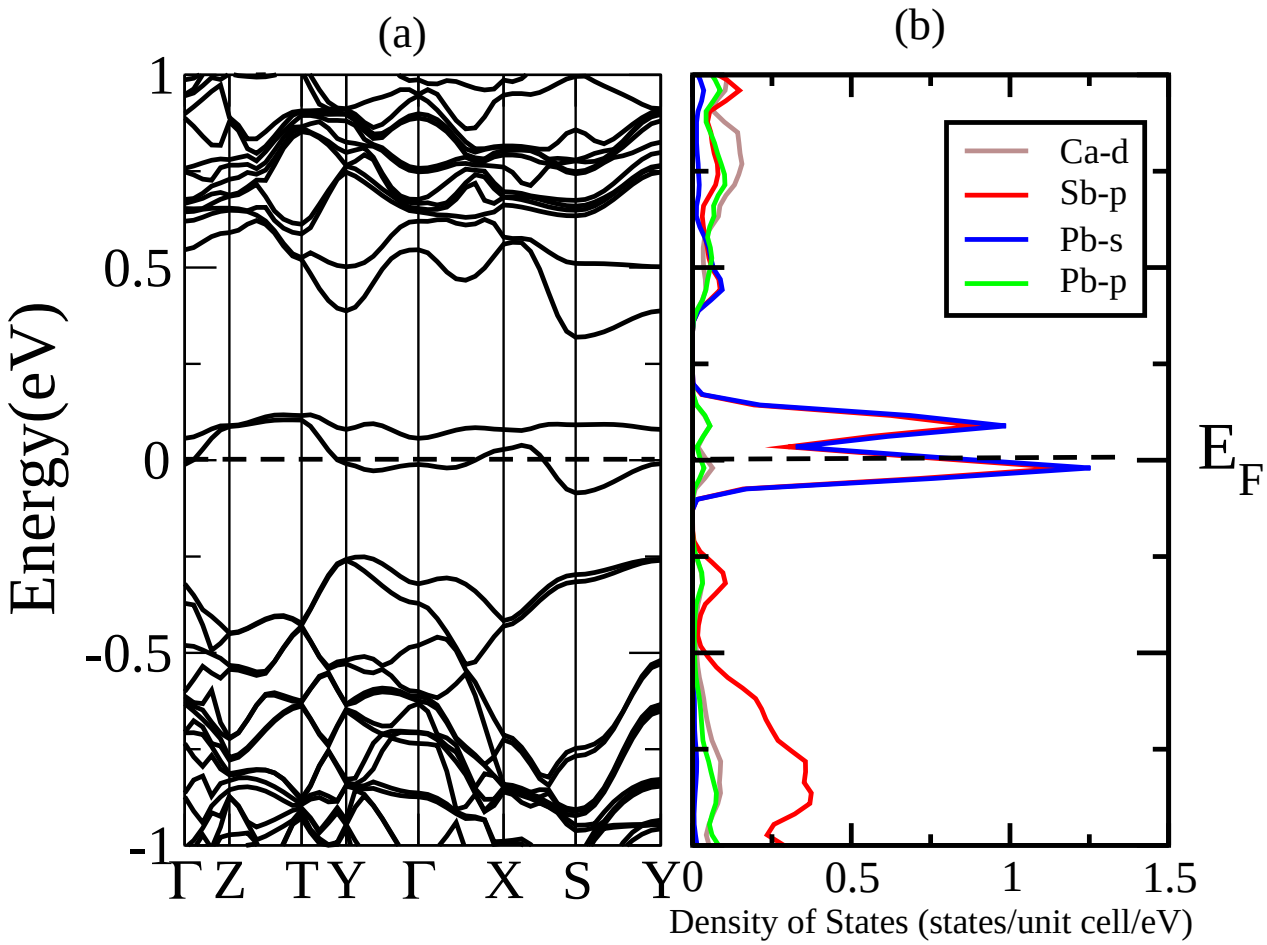

FIG. 10. (a) Calculated band structures of $Ca_5In_{1.8}Pb_{0.2}Sb_6$. (b) Calculated projected DOS for $Ca_5In_{1.8}Pb_{0.2}Sb_6$. The Fermi level is at zero.

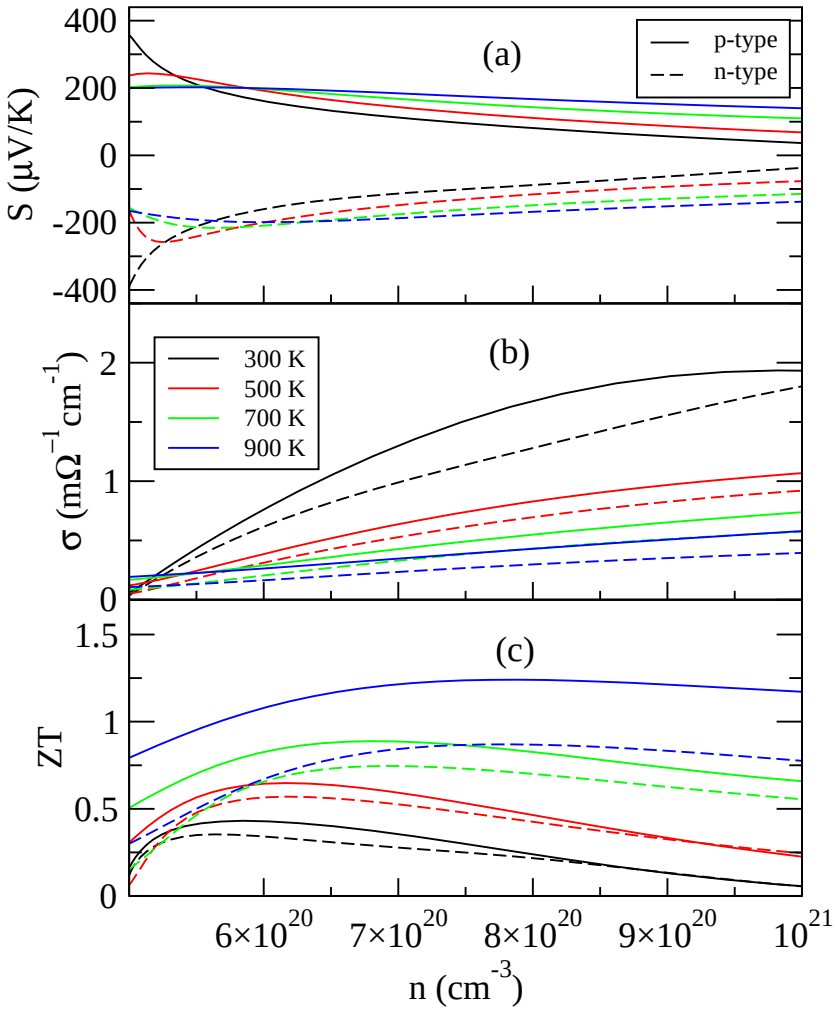

FIG. 11. Transport coefficients of p-type and n-type $Ca_5In_{1.8}Pb_{0.2}Sb_6$ as a function of carrier concentration from 5×10^{20} to 10^{21} cm^{-3} at 300 K, 500 K, 700 K, and 900 K.

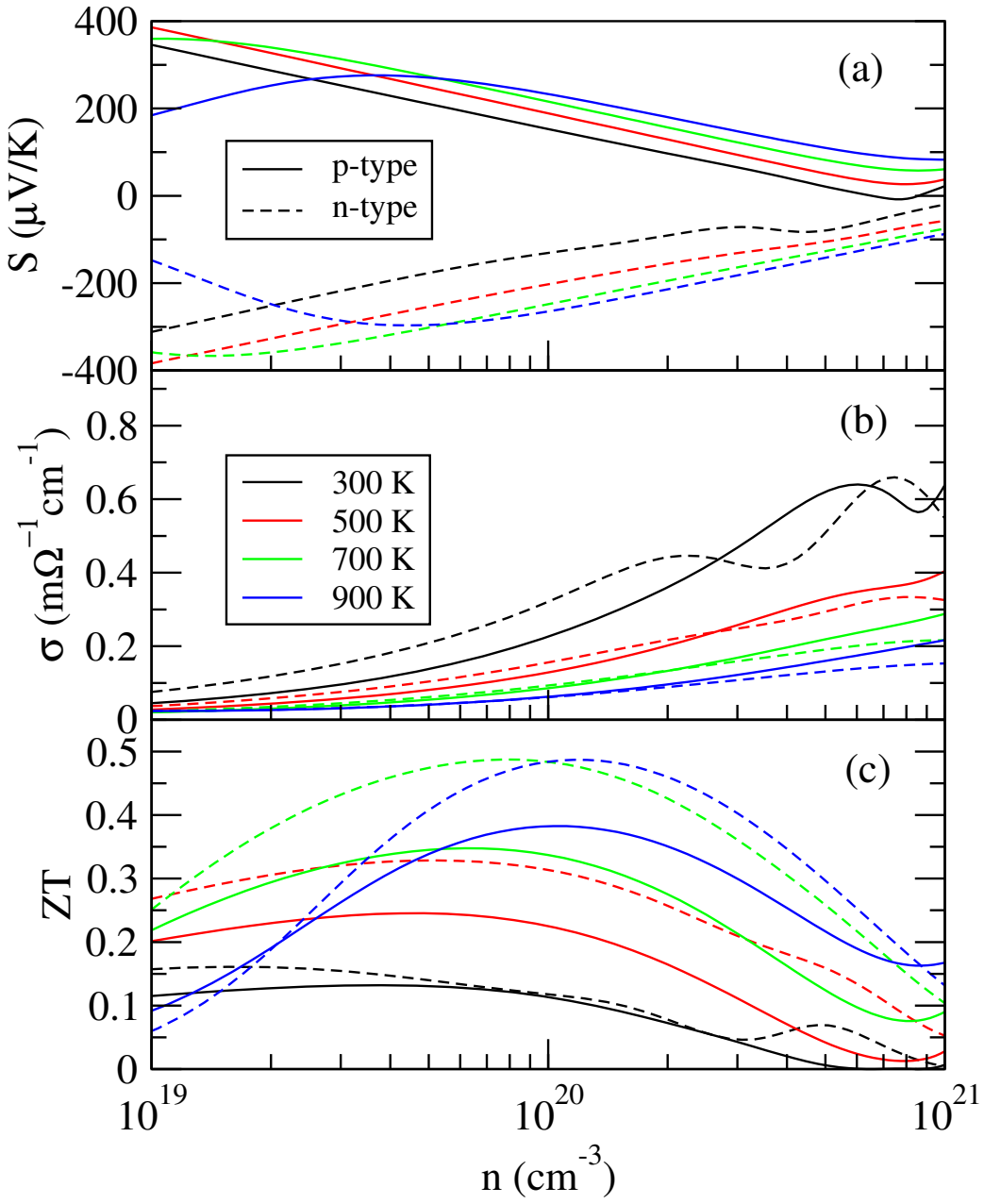

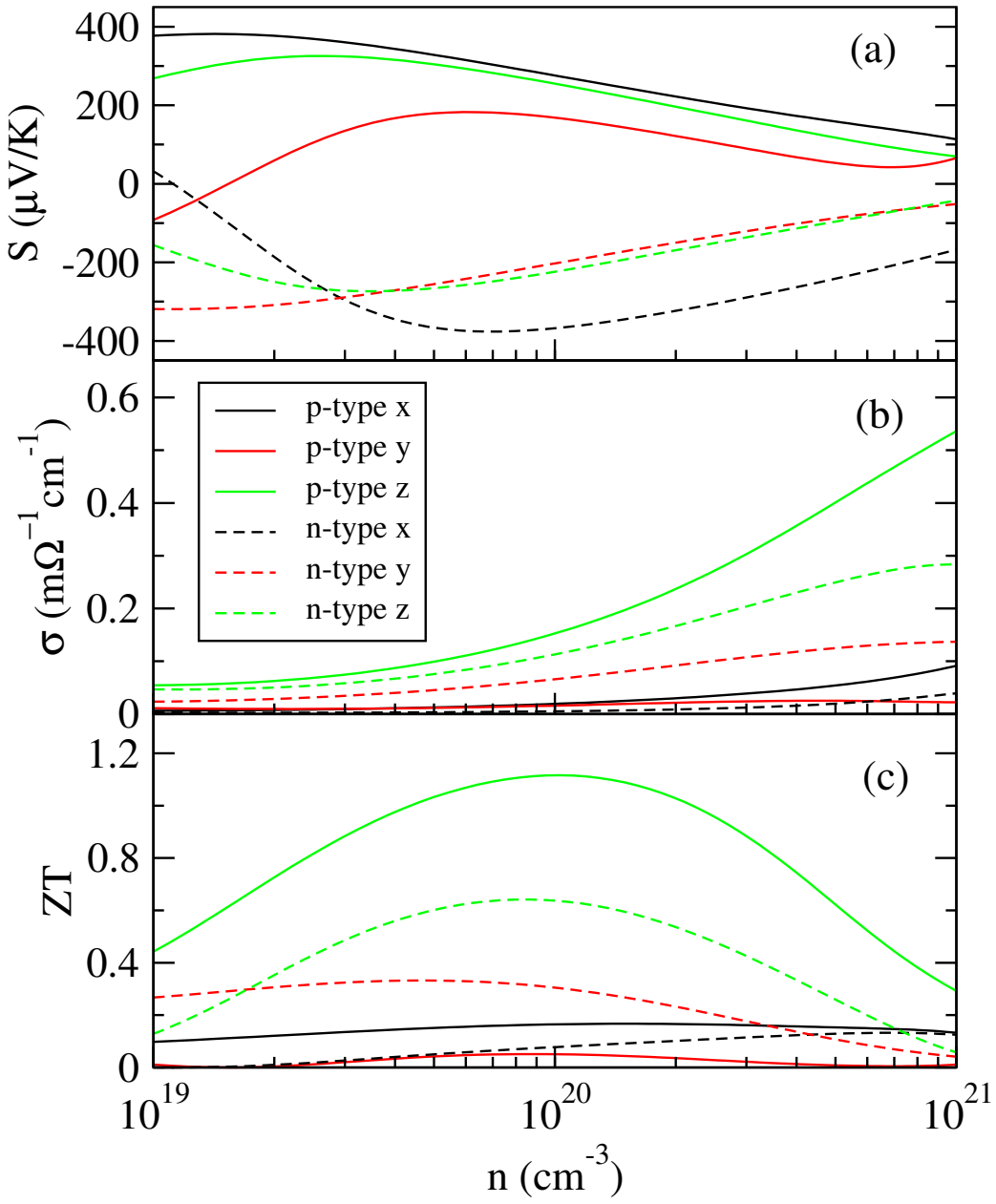

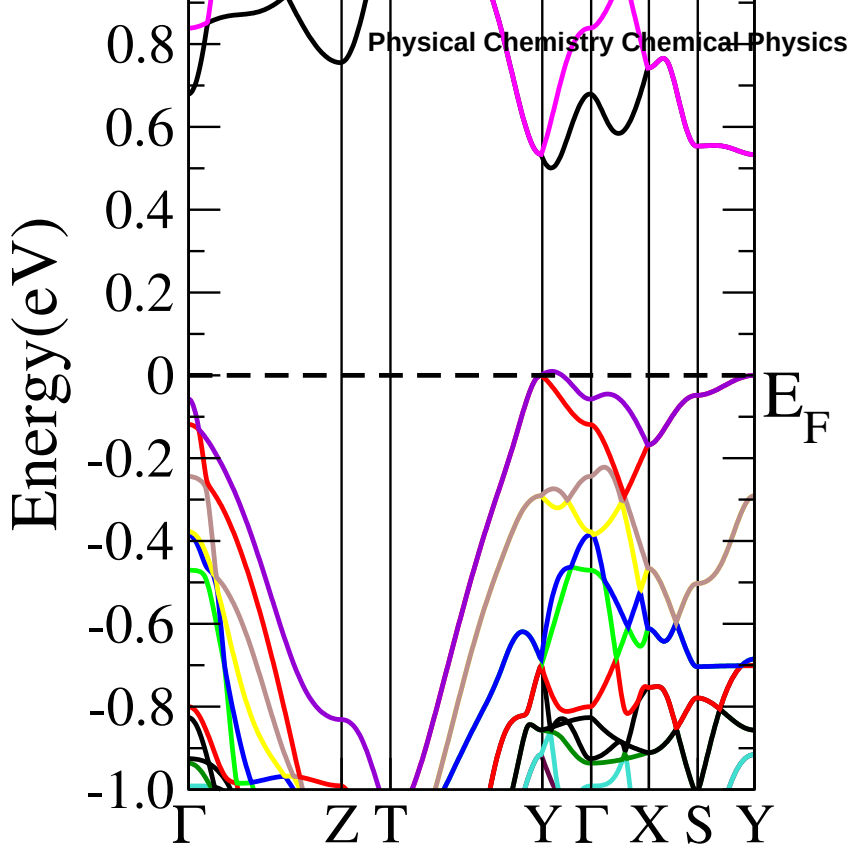

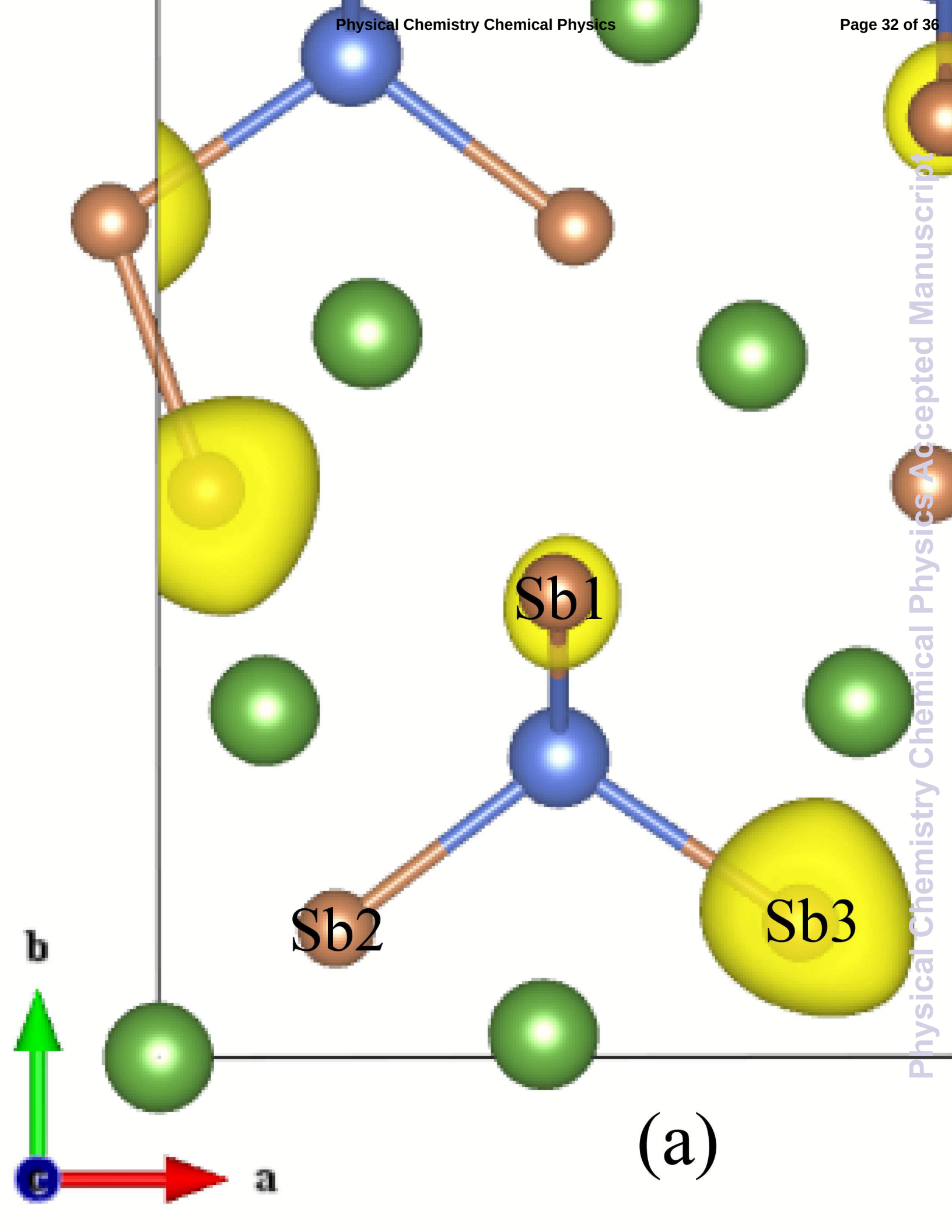

(a)